

Interpreting the 750 GeV diphoton excess in the Minimal Dilaton Model

Junjie Cao,^{1,2,*} Liangliang Shang,^{2,†} Wei Su,^{3,‡} Yang Zhang,^{3,§} and Jinya Zhu^{1,¶}

¹*Center for Theoretical Physics, School of Physics and Technology,*

Wuhan University, Wuhan 430072, China

²*Department of Physics, Henan Normal University, Xinxiang 453007, China*

³*State Key Laboratory of Theoretical Physics,*

Institute of Theoretical Physics, Academia Sinica, Beijing 100190, China

We try to interpret the 750 GeV diphoton excess in the Minimal Dilaton Model, which extends the SM by adding one linearized dilaton field and vector-like fermions. We first show by analytic formulae in this framework that the production rates of the $\gamma\gamma$, gg , $Z\gamma$, ZZ , WW^* , $t\bar{t}$ and hh signals at the 750GeV resonance are only sensitive to the dilaton-Higgs mixing angle θ_S and the parameter $\eta \equiv vN_X/f$, where f is the dilaton decay constant and N_X denotes the number of the fermions. Then we scan the two parameters by considering various theoretical and experimental constraints to find the solutions to the diphoton excess. We conclude that the model can predict the central value of the diphoton rate without conflicting with any constraints. The signatures of our explanation at the LHC Run II and the vacuum stability at high energy scale are also discussed.

PACS numbers: 12.60.Fr, 14.80.Ec, 14.65.Jk, 14.70.Bh

* junjiec@itp.ac.cn

† shllwell1988@gmail.com

‡ weisv@itp.ac.cn

§ zhangyang@itp.ac.cn

¶ zhuji@itp.ac.cn

I. INTRODUCTION

About four years ago, the hint of a 125 GeV Higgs boson was reported in the diphoton channel by both the ATLAS and CMS collaborations based on about 5 fb^{-1} data for each collaboration at the 7-TeV LHC [1, 2], and this led to the great discovery of the Higgs boson in July 2012 [3, 4]. Recently another excess in the diphoton channel was reported by the first 3.2 fb^{-1} data at the 13-TeV LHC [5, 6]. This time the invariant mass of the signal locates around 750 GeV, and its local and global significances are about 3.6σ and 2.3σ respectively for the ATLAS analysis, and 2.6σ and 2σ for the CMS analysis. Interestingly, although there exists an ostensible inconsistency in the width of the resonance ¹, both the analyses favored the diphoton production rate at about 4fb in the narrow width approximation. Such a rate is about 10^4 times larger than the prediction of the Standard Model (SM) with a 750 GeV Higgs boson [8]. Obviously, if this excess is confirmed in near future, it points undoubtedly to the existence of new physics.

So far more than one hundred theoretical papers have appeared to interpret the excess in new physics models [9–19], and most of them employed the process $gg \rightarrow S \rightarrow \gamma\gamma$ with S denoting a scalar particle with mass around 750 GeV to fit the data. From these studies, one can infer two essential ingredients of the explanations. One is that there must exist other charged and colored particles to generate by loop effects sufficiently large $S\gamma\gamma$ and Sgg interactions. The other is, given the fact that no excess was observed in the channels such as ZZ , WW^* and $t\bar{t}$ at the LHC Run I, the particle S is preferred to be gauge singlet dominated so that the branching ratios of $S \rightarrow ZZ$, WW^* , $t\bar{t}$ are not much larger than that of $S \rightarrow \gamma\gamma$. These requirements guide us in seeking for the explanations of the excess.

In this work, we consider interpreting the diphoton excess in the Minimal Dilaton Model (MDM), which extends the SM by one gauge singlet field called dilaton [20–22]. Just like the traditional dilaton theories [23], the dilaton in this model arises from a strong interaction theory with approximate scale invariance at a certain high energy scale. The breakdown of the invariance then triggers the electroweak symmetry breaking, and during this process, the dilaton as the pseudo Nambu-Goldstone particle of the broken invariance can be naturally light in comparison with the high energy scale. Furthermore, this model assumes that all SM particles except for the Higgs field do not interact with the dynamics sector, and consequently the dilaton does not couple directly to the fermions and W , Z bosons in the SM. In this sense, the dilaton is equivalent to an

¹ Currently with insufficient experimental data, the ATLAS analysis slightly preferred a wide width of the resonance (about 45 GeV) to a narrow width [5], and by contrast the CMS analysis favored a narrow width [6]. Very recently, an analysis by combining both the ATLAS data and the CMS data was carried out, and it indicated that the narrow width was preferred [7].

electroweak gauge singlet field. The model also consists of massive vector-like fermions acting as the lightest particles in the dynamical sector, to which the dilaton naturally couples in order to recover the scale invariance: $M \rightarrow Me^{-\phi/f}$. As a result, the interactions between the dilaton and the photons/gluons are induced through loop diagrams of these fermions. These characters enable the MDM as a hopeful theory to explain the diphoton excess through the dilaton production. Discussing the capability of the MDM in explaining the excess is the aim of this work.

This paper is organized as follows. We first introduce briefly the MDM in Section II, and present in Section III some analytical formulae which are used to calculate the diphoton rate. In Section IV, we discuss the constraints on the model, its capability in explaining the excess, and also the related phenomenology at the LHC Run II. For completeness, in section V we turn to discuss the vacuum stability at high energy scale. Finally, we draw our conclusions in Section VI.

II. THE MINIMAL DILATON MODEL

As introduced in last section, the MDM extends the SM by adding one gauge singlet field S , which represents a linearized dilaton field, and also vector-like fermions X_i . The low energy effective Lagrangian is then written as [20, 21]

$$\mathcal{L} = \mathcal{L}_{\text{SM}} + \frac{1}{2} \partial_\mu S \partial^\mu S + \sum_{i=1}^{N_X} \bar{X}_i \left(i \not{D} - \frac{M_i}{f} S \right) X_i - V(S, \tilde{H}), \quad (1)$$

where \mathcal{L}_{SM} is the SM Lagrangian without Higgs potential, f is the decay constant of the dilaton S , M_i is the mass of the fermion X_i , and N_X is the number of the vector-like fermions. The scalar potential $V(S, \tilde{H})$ contains terms with explicit breaking of the scale invariance, and its general form is given by

$$V(S, \tilde{H}) = \frac{m_S^2}{2} S^2 + \frac{\lambda_S}{4} S^4 + m_H^2 |\tilde{H}|^2 + \lambda_H |\tilde{H}|^4 + \frac{\lambda_{HS}}{2} S^2 |\tilde{H}|^2, \quad (2)$$

where m_S , λ_S , m_H , λ_H and λ_{HS} are all free real parameters.

About the Lagrangian in Eq.(1), one should note following points:

- The MDM is actually a low energy theoretical framework describing the breakdown of a UV strong dynamics with approximate scale invariance, and the dilaton in this theory is distinguished from the usual one. Explicitly speaking, in the traditional dilaton models the whole SM sector is usually assumed to be a part of the strong dynamics, and all the fermions and gauge bosons of the SM are composite particles at the weak scale [23]. Under

these theoretical assumptions, the couplings of the linearized dilaton S to the SM fields take following form [23]

$$\mathcal{L} = \frac{S}{f} T_\mu^\mu, \quad (3)$$

where T_μ^μ represents the trace of the energy-momentum tensor of the SM. Through the interactions in Eq.(3), the dilaton couples directly to the fermions and W, Z bosons in the SM with the strengthes proportional to the mass of the involved particle. In this way, the dilaton mimics the properties of the SM Higgs boson. By contrast, in the MDM all SM particles except for the Higgs field are assumed to be the spectators of the strong dynamics, and they are all elementary particles. As a result, the dilaton does not couple directly to these particles.

- In the original version of the MDM, the authors set $N_X = 1$ and chose the quantum numbers of the fermion X_i same as those of the right-handed top quark. This setting was motivated by topcolor theory [24], which intended to present a reasonable explanation of the relatively large top quark mass within a minimal framework. However, as we will show below, such a setting is tightly limited by the vacuum stability of the theory at m_{X_i} scale in interpreting the diphoton excess. Considering that a strong dynamical theory usually involves rich fermion fields and the assignment on their quantum numbers is somewhat arbitrary, we therefore consider a more general but also simple case, which assumes that all the vector-like fermions are identical, and each of them transforms in the $(3, 1, Y = 2Q_X)$ representation of the SM gauge group $SU(3)_c \otimes SU(2)_L \otimes U(1)_Y$. In the following, we vary the number of the fermions N_X , their common mass m_X , and also their electric charge Q_X to discuss the diphoton excess.

If one writes the Higgs field in unitary gauge via $\tilde{H} = \frac{1}{\sqrt{2}}U(0, H)^T$, the scalar potential in Eq.(2) can be rewritten as

$$\tilde{V}(S, H) = \frac{m_S^2}{2}S^2 + \frac{\lambda_S}{4}S^4 + \frac{m_H^2}{2}H^2 + \frac{\lambda_H}{4}H^4 + \frac{\lambda_{HS}}{4}S^2H^2. \quad (4)$$

In the following, we consider the most general situation in which both H and S take vacuum expectation values (VEV), $\langle H \rangle = v$ and $\langle S \rangle = f$, and they mix to form mass eigenstates h and s :

$$\begin{aligned} h &= \cos \theta_S H + \sin \theta_S S, \\ s &= -\sin \theta_S H + \cos \theta_S S. \end{aligned} \quad (5)$$

In our scheme for the diphoton excess, h corresponds to the 125 GeV Higgs boson discovered at the LHC, and s is responsible for the 750GeV diphoton excess by the process $gg \rightarrow s \rightarrow \gamma\gamma$. So in the following, we set $m_h = 125\text{GeV}$, $m_s = 750\text{GeV}$ and $v = 246\text{GeV}$, and for the convenience of our discussion, we choose $\eta \equiv \frac{v}{f}N_X$, $\sin\theta_S$, Q_X , N_X and m_X as the input parameters of the MDM model. In this case, we have following relations

$$\begin{aligned}\lambda_{HS} &= \frac{2\eta(m_h^2 - m_s^2) \sin\theta_S \cos\theta_S}{v^2 N_X}, \\ \lambda_H &= \frac{m_h^2 \cos^2\theta_S + m_s^2 \sin^2\theta_S}{2v^2}, \\ \lambda_S &= \frac{\eta^2(m_h^2 \sin^2\theta_S + m_s^2 \cos^2\theta_S)}{2v^2 N_X^2}.\end{aligned}\tag{6}$$

With the assumption that the dilaton is fully responsible for the fermion masses, the Yukawa coupling of X_i is given by $y_X \equiv \frac{m_X}{f} = \frac{\eta m_X}{v N_X}$. Obviously y_X is inversely proportional to N_X for fixed η and m_X . As we will show below, the diphoton rate is only sensitive to the parameters η , $\sin\theta_S$ and Q_X , and does not depend on y_X directly.

III. USEFUL FORMULAE IN GETTING THE DIPHOTON EXCESS

In the MDM, the particle s may decay into gg , $\gamma\gamma$, $Z\gamma$, ZZ , WW^* , $f\bar{f}$ and hh . In this section, we list the formulae for the widths of these decays, which are needed to get the diphoton rate. As we will show below, these formulae are helpful to understand our results.

- The widths of $\phi \rightarrow \gamma\gamma, gg, Z\gamma$ with $\phi = h, s$:

$$\Gamma_{\phi \rightarrow \gamma\gamma} = \frac{G_\mu \alpha^2 m_\phi^3}{128\sqrt{2}\pi^3} |I_\gamma^\phi|^2,\tag{7}$$

$$\Gamma_{\phi \rightarrow gg} = \frac{G_\mu \alpha_s^2 m_\phi^3}{16\sqrt{2}\pi^3} |I_g^\phi|^2,\tag{8}$$

$$\Gamma_{\phi \rightarrow Z\gamma} = \frac{G_\mu^2 m_W^2 \alpha m_\phi^3}{64\pi^4} \left(1 - \frac{m_Z^2}{m_\phi^2}\right)^3 |I_{Z\gamma}^\phi|^2,\tag{9}$$

where the I_g^ϕ , I_γ^ϕ and $I_{Z\gamma}^\phi$ are given by

$$I_\gamma^h = \cos\theta_S \times (A_1(\tau_W) + \frac{4}{3}A_{\frac{1}{2}}(\tau_t)) + \sin\theta_S N_c \eta Q_X^2 A_{\frac{1}{2}}(\tau_X),\tag{10}$$

$$I_\gamma^s = -\sin\theta_S \times (A_1(\tau_W) + \frac{4}{3}A_{\frac{1}{2}}(\tau_t)) + \cos\theta_S N_c \eta Q_X^2 A_{\frac{1}{2}}(\tau_X),\tag{11}$$

$$I_g^h = \frac{\cos\theta_S}{2} \times A_{\frac{1}{2}}(\tau_t) + \frac{\eta \sin\theta_S}{2} A_{\frac{1}{2}}(\tau_X),\tag{12}$$

$$I_g^s = -\frac{\sin\theta_S}{2} \times A_{\frac{1}{2}}(\tau_t) + \frac{\eta \cos\theta_S}{2} A_{\frac{1}{2}}(\tau_X),\tag{13}$$

$$\begin{aligned}
I_{Z\gamma}^h &= \cos\theta_S \times (\cos\theta_W C_1(\tau_W^{-1}, \eta_W^{-1}) + \frac{2(1 - \frac{8}{3}\sin^2\theta_W)}{\cos\theta_W} C_{\frac{1}{2}}(\tau_t^{-1}, \eta_t^{-1})) \\
&\quad + 4\sin\theta_S N_c \eta Q_X^2 \frac{\sin^2\theta_W}{\cos\theta_W} C_{\frac{1}{2}}(\tau_X^{-1}, \eta_X^{-1}), \tag{14}
\end{aligned}$$

$$\begin{aligned}
I_{Z\gamma}^s &= -\sin\theta_S \times (\cos\theta_W C_1(\tau_W^{-1}, \eta_W^{-1}) + \frac{2(1 - \frac{8}{3}\sin^2\theta_W)}{\cos\theta_W} C_{\frac{1}{2}}(\tau_t^{-1}, \eta_t^{-1})) \\
&\quad + 4\cos\theta_S N_c \eta Q_X^2 \frac{\sin^2\theta_W}{\cos\theta_W} C_{\frac{1}{2}}(\tau_X^{-1}, \eta_X^{-1}). \tag{15}
\end{aligned}$$

In above expressions, $A_{\frac{1}{2}}$, A_1 , $C_{\frac{1}{2}}$, C_1 are the loop functions defined in [25] with $\tau_\beta = m_\phi^2/(4m_\beta^2)$ and $\eta_\beta = m_Z^2/(4m_\beta^2)$ for $\beta = W, t, X_i$.

About these formulae, one should note that the terms proportional to $\cos\theta_S$ in the expressions of I_i^s are contributed by the dilaton component of s , while those proportional to $\sin\theta_S$ come from the H -component of s . One should also note that in the case of $\sin\theta_S \sim 0$, which is required by the null excess in the channels such as ZZ and hh at the 750GeV invariant mass (see below) and also by the 125GeV Higgs data, I_γ^s , I_g^s and $I_{Z\gamma}^s$ are all dominated by the contribution from the vector-like fermions, and consequently they are correlated. Explicitly speaking, we have $I_\gamma^s : I_g^s : I_{Z\gamma}^s = N_c Q_X^2 : \frac{1}{2} : \frac{N_c Q_X^2}{2} \frac{\sin^2\theta_W}{\cos\theta_W}$ in the limit $m_s, m_X \gg m_Z$. This correlation may sever as a test of the model at future LHC experiments.

- The widths of the decays $s \rightarrow VV^*$ with $V = W, Z$.

If one parameterizes the effective sVV^* interaction as

$$\mathcal{A}_{sVV^*} = g_V m_V (A_V^s g^{\mu\nu} + B_V^s p_2^\mu p_1^\nu) \epsilon_\mu(p_1) \epsilon_\nu(p_2),$$

then the decay width of $s \rightarrow VV^*$ is given by[13]

$$\begin{aligned}
\Gamma_{s \rightarrow VV^*} &= \delta_V \frac{G_F m_s^3}{16\pi\sqrt{2}} \frac{4m_V^4}{m_s^4} \sqrt{\lambda(m_V^2, m_V^2; m_s^2)} \times \\
&\quad \left[A_V^s A_V^{s*} \times \left(2 + \frac{(p_1 \cdot p_2)^2}{m_V^4} \right) + (A_V^s B_V^{s*} + A_V^{s*} B_V^s) \times \left(\frac{(p_1 \cdot p_2)^3}{m_V^4} - p_1 \cdot p_2 \right) \right. \\
&\quad \left. + B_V^s B_V^{s*} \times \left(m_V^4 + \frac{(p_1 \cdot p_2)^4}{m_V^4} - 2(p_1 \cdot p_2)^2 \right) \right], \tag{16}
\end{aligned}$$

where $\delta_V = 2(1)$ for $V = W(Z)$ respectively and $\lambda(x, y, z) = ((z - x - y)^2 - 4xy)/z^2$.

In the MDM, we have

$$\begin{aligned}
A_W^s &\simeq -\sin\theta_S, \quad B_W^s \simeq 0, \\
A_Z^s &\simeq -\sin\theta_S + \frac{\alpha}{4\pi m_Z^2} \cos\theta_S N_c \eta Q_X^2 \tan^2\theta_W p_1 \cdot p_2 A_{\frac{1}{2}}(\tau_X), \\
B_Z^s &\simeq -\frac{\alpha}{4\pi m_Z^2} \cos\theta_S N_c \eta Q_X^2 \tan^2\theta_W A_{\frac{1}{2}}(\tau_X).
\end{aligned}$$

Note that in the expressions of A_Z^s and B_Z^s , we have included the one-loop corrections. This is because in case of $\sin\theta_S \sim 0$, the corrections are not always smaller than the tree level contributions. Also note that in getting A_Z^s and B_Z^s , to a good approximation we have neglected the Z boson mass appeared in the loop functions, and that is why we can express the corrections in term of the simple function $A_{\frac{1}{2}}(\tau_X)$.

- The width of the tree-level decay $s \rightarrow f\bar{f}$ with f denoting any of the fermions in the SM:

$$\Gamma_{s \rightarrow f\bar{f}} = \sin^2\theta_S \frac{3G_\mu m_f^2 m_s}{4\sqrt{2}\pi} \left(1 - \frac{4m_f^2}{m_s^2}\right)^{\frac{3}{2}}. \quad (17)$$

Note that for this kind of decays, the widths are proportional to $\sin^2\theta_S$.

- The width of the tree level decay $s \rightarrow hh$:

$$\Gamma_{s \rightarrow hh} = \frac{|C_{shh}|^2}{16\pi m_s^2} \left(\frac{m_s^2}{4} - m_h^2\right)^{\frac{1}{2}}, \quad (18)$$

where

$$\begin{aligned} C_{shh} &= -6\lambda_H v \sin\theta_S \cos^2\theta_S + 6\lambda_S f \sin^2\theta_S \cos\theta_S \\ &\quad + \lambda_{HS}(-v \sin^3\theta_S + f \cos^3\theta_S - 2f \sin^2\theta_S \cos\theta_S + 2v \sin\theta_S \cos^2\theta_S) \\ &\simeq -\frac{2m_s^2}{v} \sin\theta_S. \end{aligned}$$

In getting the final expression of C_{shh} , we have used the relation $m_s^2 \gg m_h^2$ and $\sin\theta_S \sim 0$ to neglect some unimportant terms. Just like the decays $s \rightarrow WW^*$ and $s \rightarrow t\bar{t}$, $\Gamma_{s \rightarrow hh}$ is proportional to $\sin^2\theta_S$.

With these formulae, the total width of the scalar s and the s -induced diphoton rate can be written as

$$\Gamma_{tot} = \Gamma_{s \rightarrow gg} + \Gamma_{s \rightarrow \gamma\gamma} + \Gamma_{s \rightarrow Z\gamma} + \Gamma_{s \rightarrow ZZ} + \Gamma_{s \rightarrow WW^*} + \Gamma_{s \rightarrow f\bar{f}} + \Gamma_{s \rightarrow hh} + \Gamma_{new}, \quad (19)$$

$$\sigma_{\gamma\gamma}^{13TeV} = \frac{\Gamma_{\phi \rightarrow gg}}{\Gamma_{H \rightarrow gg}^{SM}} \Big|_{m_H \simeq 750\text{GeV}} \times \sigma_{\sqrt{s}=13\text{TeV}}^{SM}(H) \times \frac{\Gamma_{s \rightarrow \gamma\gamma}}{\Gamma_{tot}}, \quad (20)$$

where the Γ_{new} in Eq.(19) represents the contribution from the exotic decays of s , which may exist if the MDM is embedded in a more complex theoretical framework, $\Gamma_{H \rightarrow gg}^{SM}$ denotes the decay width of the SM Higgs H into gg with $m_H = 750\text{GeV}$, and $\sigma_{\sqrt{s}=13\text{TeV}}^{SM}(H) = 735\text{fb}$ is the NNLO

production rate of the H at the 13 TeV LHC [29]. Obviously, if Γ_{tot} is determined mainly by Γ_{gg} , the rate can be approximated by

$$\sigma_{\gamma\gamma}^{13TeV} \simeq \frac{\Gamma_{\phi \rightarrow \gamma\gamma}}{\Gamma_{H \rightarrow gg}^{SM}} \Big|_{m_H \simeq 750 \text{ GeV}} \times \sigma_{\sqrt{s}=13 \text{ TeV}}^{SM}(H) \propto \eta^2 Q_X^4, \quad (21)$$

while if Γ_{tot} takes a fixed value, we have

$$\sigma_{\gamma\gamma}^{13TeV} = \left(\frac{45 \text{ GeV}}{\Gamma_{tot}} \right) \times \sigma_{norm} \times (\eta Q_X)^4, \quad (22)$$

where the normalized cross section σ_{norm} is equal to 0.019 fb (0.018 fb) for $m_X = 1 \text{ TeV}$ (1.5 TeV).

From the discussion in this section, one can get following important conclusions:

- The widths of $s \rightarrow gg, \gamma\gamma, Z\gamma$ or the production rates of the $gg, \gamma\gamma$ and $Z\gamma$ signals at the LHC are correlated by

$$\Gamma_{s \rightarrow gg} : \Gamma_{s \rightarrow \gamma\gamma} : \Gamma_{s \rightarrow Z\gamma} \simeq 1 : \frac{9 \alpha^2}{2 \alpha_s^2} Q_X^4 : \frac{9 \alpha^2}{4 \alpha_s^2} \tan^2 \theta_W Q_X^4 \simeq 1 : 0.03 Q_X^4 : 0.004 Q_X^4. \quad (23)$$

- The widths listed from Eq.(7) to Eq.(18) depend on the number of the vector-like fermions N_X only through the parameter $\eta \equiv \frac{v N_X}{f}$. As a result, explaining the diphoton excess puts non-trivial requirements on the combination $\frac{v N_X}{f}$, instead of on the individual parameter N_X or $y_X = \frac{\eta m_X}{v N_X}$.
- Since the recent LHC searches for right-handed heavy quarks have required $m_X \gtrsim 900 \text{ GeV}$ [26–28] and thus $\tau_X \equiv m_s^2 / (4m_X^2) < 0.2$, the loop functions appeared in the widths change slightly with the further increase of m_X . This implies that the widths and also the cross section have a very weak dependence on the value of m_X . As a result, the results obtained in this work are only sensitive to the parameters $\eta, \sin \theta_S$ and Q_X .

At this stage, one can infer that the parameter N_X may also be understood as the total number of the vector-like fermions with the electric charge Q_X in the strong dynamics because the contributions of the fermions to the diphoton rate are roughly identical. Since the particle content of a strong dynamics is usually rich, N_X is naturally larger than 1.

We remind that the second and third conclusions depend on the assumption that the dilaton is fully responsible for the masses of the vector-like fermions, and within our knowledge, they were not paid attention to in previous literatures.

TABLE I. Upper limits on various 750GeV resonant signals at 8-TeV LHC set by either ATLAS or CMS collaboration [13].

Channel	jj [35, 36]	hh [37–40]	WW^* [41, 42]	ZZ [41, 43]	$Z\gamma$ [44]	$t\bar{t}$ [45, 46]
95% C.L. limits	1800 fb	35 fb	37 fb	12 fb	3.6 fb	450 fb

IV. NUMERICAL RESULTS AND DISCUSSIONS

In this section, we discuss the diphoton excess in the MDM. In order to get the favored parameter space for the excess, we fix $Q_X = \frac{2}{3}, \frac{5}{3}$ and $m_X = 1\text{TeV}, 1.5\text{TeV}$ at each time, and scan following parameter space

$$0 < \eta \leq 2, \quad |\tan \theta_S| \leq 0.1. \quad (24)$$

During the scan, we consider following theoretical and experimental constraints:

- The vacuum stability at the scale of $m_s = 750\text{GeV}$ for the scalar potential, which corresponds to the requirement $4\lambda_H\lambda_S - \lambda_{HS}^2 > 0$ [20].
- Constraints from the perturbativity at the scale of $m_s = 750\text{GeV}$, which requires $\lambda_S, \lambda_H, \lambda_{HS} \lesssim 4\pi$, and $y_X \lesssim 4\pi/\sqrt{N_c}$ [18].
- Constraints from the electroweak precision data. We calculate the Peskin-Takeuchi S and T parameters [30] with the formulae presented in [20], and construct χ_{ST}^2 by following experimental fit results with $m_{h,ref} = 125$ GeV and $m_{t,ref} = 173$ GeV [31]:

$$S = 0.06 \pm 0.09, \quad T = 0.10 \pm 0.07, \quad \rho_{ST} = 0.91. \quad (25)$$

In our calculation, we require that the samples satisfy $\chi_{ST}^2 \leq 6.18$.

- Experimental constraints from the 125 GeV Higgs data, which include the updated exclusive signal rates for $\gamma\gamma, ZZ^*, WW^*, b\bar{b}$ and $\tau\bar{\tau}$ channels [32, 33]. We perform the fits like our previous paper [22, 34], and require the samples to coincide with the combined data at 2σ level.
- Experimental constraints from the null results in the search for the 750 GeV resonance through other channels such as $s \rightarrow ZZ, hh$ at Run I, just like what we did in [13]. The upper bounds on these channels at 95% C.L. are listed in Table I.

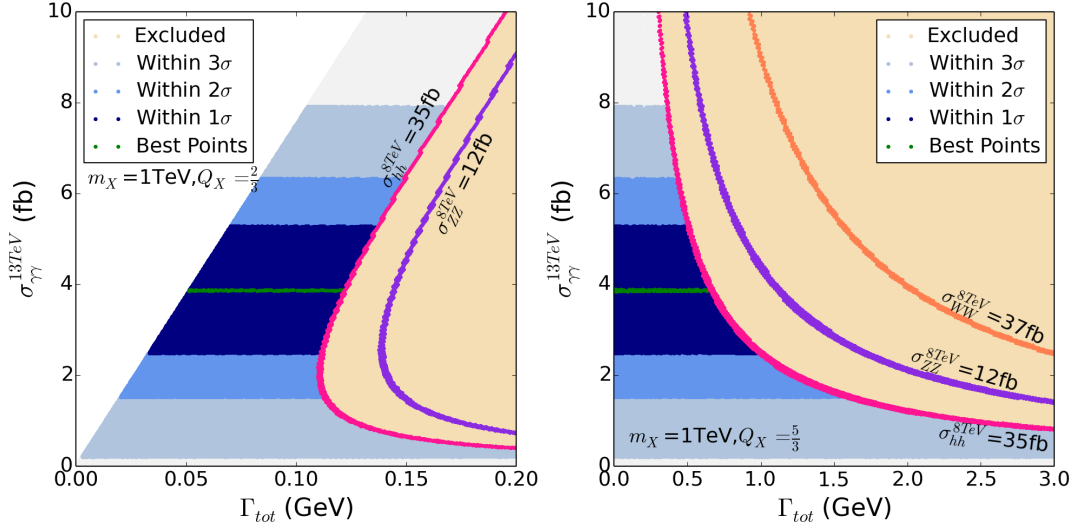


FIG. 1. The fit results of the MDM to the 750 GeV diphoton data together with the LHC Run I constraints listed in Table I, which are projected on the $\sigma_{\gamma\gamma}^{13TeV} - \Gamma_{tot}$ planes for $Q_X = 2/3$ (left panel) and $Q_X = 5/3$ (right panel) respectively. The regions filled by the colors from gray to deep blue represent the parameter spaces that can fit the diphoton data within 3σ , 2σ and 1σ level respectively, and by contrast the regions covered by straw color are excluded by the constraints. The boundaries for the hh , ZZ and WW^* channels are also plotted, which correspond to blue lines, red lines and brown lines respectively, and the other constraints listed in Table I are too weak to be drawn on the panels. In each panel, the green line represents the best-fit samples. In getting this panel, we have set $\Gamma_{new} = 0$ and $m_X = 1\text{TeV}$, and we checked that $m_X = 1.5\text{TeV}$ predicts roughly same results, which reflects that our results are insensitive to m_X .

For each sample surviving the constraints, we perform a fit to the 750 GeV diphoton data collected at the 8 TeV and the 13 TeV LHC. In doing this, we use the method introduced in [9], where the data were given by

$$\mu_i^{exp} = \sigma(pp \rightarrow \gamma\gamma) = \begin{cases} 0.63 \pm 0.25 \text{ fb} & \text{CMS at } \sqrt{s} = 8 \text{ TeV}, \\ 0.46 \pm 0.85 \text{ fb} & \text{ATLAS at } \sqrt{s} = 8 \text{ TeV}, \\ 5.6 \pm 2.4 \text{ fb} & \text{CMS at } \sqrt{s} = 13 \text{ TeV}, \\ 6.2^{+2.4}_{-2.0} \text{ fb} & \text{ATLAS at } \sqrt{s} = 13 \text{ TeV}, \end{cases} \quad (26)$$

and the $\chi_{\gamma\gamma}^2$ function was given by [9, 13]

$$\chi^2 = \sum_{i=1}^4 \chi_i^2, \quad \chi_i^2 = \begin{cases} 2[\mu_i^{exp} - \mu_i + \mu_i \ln \frac{\mu_i}{\mu_i^{exp}}] & \text{for the 13 TeV ATLAS data,} \\ \frac{(\mu_i^{exp} - \mu_i)^2}{\sigma_{\mu_i^{exp}}^2} & \text{for the other three sets of data,} \end{cases} \quad (27)$$

with μ_i denoting the theoretical prediction of the diphoton rate.

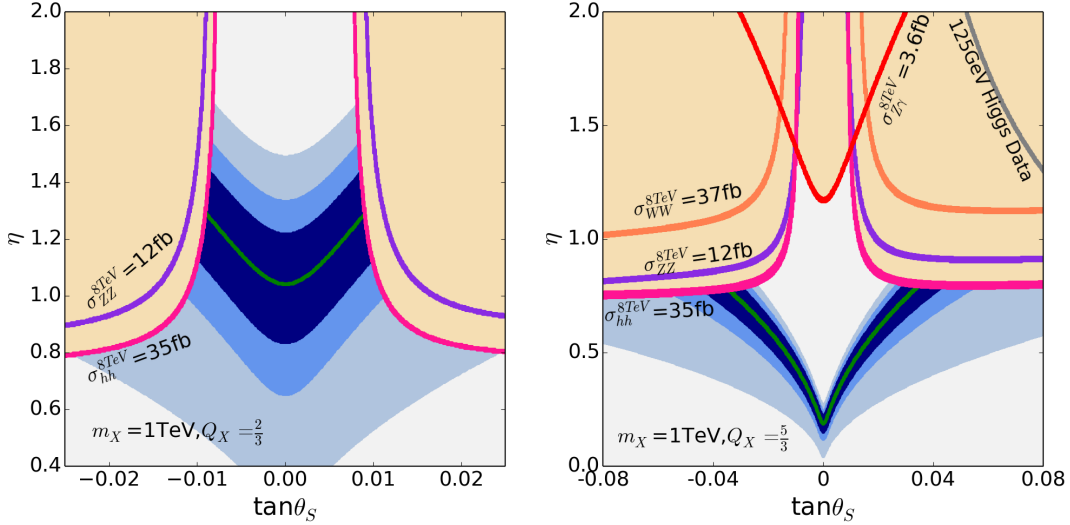


FIG. 2. Same samples as those in Fig.1, but projected on the $\eta - \tan\theta_S$ planes. Although we take $m_X = 1\text{TeV}$ in getting this figure, we check that setting $m_X = 1.5\text{TeV}$ produces indistinguishable difference on the figure due to the comments below Eq.(23).

In the following, we only consider the samples surviving the first four constraints. In Fig.1, we project these samples on the $\sigma_{\gamma\gamma}^{13\text{TeV}} - \Gamma_{tot}$ planes for $Q_X = 2/3$ (left panel) and $Q_X = 5/3$ (right panel) respectively. The details of this figure are explained in its caption. From this figure, one can get following facts:

- The central value of the diphoton rate is 3.9fb at the 13TeV LHC from the fit, and the 1σ , 2σ and 3σ ranges of the rate are (2.5 ~ 5.3) fb, (1.5 ~ 6.3) fb, (0.2 ~ 7.9) fb respectively. Note that this conclusion is independent of the value of Q_X .
- For both $Q_X = \frac{2}{3}$ and $Q_X = \frac{5}{3}$ cases, the diphoton excess can be well explained. The difference of the two options comes from the fact that for $Q_X = \frac{2}{3}$ case, $\Gamma_{tot} \lesssim 0.15\text{GeV}$ if one wants to explain the excess at 2σ level, while for $Q_X = \frac{5}{3}$ case, $\Gamma_{tot} \lesssim 1.6\text{GeV}$. The reason for such a difference is that in the $Q_X = \frac{5}{3}$ case, $\sin\theta_S$ can take a larger value (see discussion below).
- Among the channels listed in Table I, the hh channel puts the tightest constraints on the parameter space regardless the value of Q_X .

Next we illustrate the favored parameter regions for the excess. For this purpose, we project the samples used in Fig.1 on the $\eta - \tan\theta_S$ planes, which are shown in Fig.2. This figure indicates following facts:

TABLE II. Detailed information for one of the best points in the left and right panels of Fig.2 (labeled by P1 and P2 hereafter) respectively. We checked that all these points predict $\chi^2_{\gamma\gamma} = 2.32$, which corresponds to a p -value of 0.68.

Point	Q_X	η	$\tan\theta_S$	$\frac{\Gamma_{\phi \rightarrow gg}}{\Gamma_{H \rightarrow gg}^{SM}}$	$\text{BR}_{\phi \rightarrow gg}$	$\text{BR}_{\phi \rightarrow \gamma\gamma}$	$\text{BR}_{\phi \rightarrow ZZ}$	$\text{BR}_{\phi \rightarrow WW^*}$	$\text{BR}_{\phi \rightarrow hh}$	$\text{BR}_{\phi \rightarrow t\bar{t}}$
P_1	$\frac{2}{3}$	1.144	-0.005	0.973	82.1%	0.54%	2.4%	4.85%	9.00%	1.02%
P_2	$\frac{5}{3}$	0.336	-0.005	0.083	24.4%	6.34%	9.62%	19.23%	35.60%	4.05%

- In order to explain the diphoton excess at 2σ level, $0.65 \leq \eta \leq 1.55$ and $|\tan\theta_S| \leq 0.012$ are preferred for $Q_X = \frac{2}{3}$ case, and by contrast $0.15 \leq \eta \leq 0.8$ and $|\tan\theta_S| \leq 0.06$ are preferred for $Q_X = \frac{5}{3}$ case. Note that in the $Q_X = \frac{5}{3}$ case, a smaller η as well as a wider range of $\tan\theta_S$ are favored to explain the excess in comparison with the $Q_X = \frac{2}{3}$ case. The reason is that a larger Q_X can increase greatly the width and also the branching ratio of $s \rightarrow \gamma\gamma$, which in return needs a smaller s production rate to explain the excess.
- The channels listed in Table I exclude the parameter space characterized by a large η and/or a large $|\tan\theta_S|$. For these cases, the production rates of the channels are usually enhanced, which can be inferred from the expressions of the widths.
- In case of $\tan\theta_S \simeq 0$, the $Z\gamma$ channel may impose upper bounds on η , which is shown in the right panel of Fig.2.
- The favored parameter space is not symmetric if the sign for $\tan\theta_S$ is reversed, and this asymmetry turns out to be more obvious for larger Q_X and $|\tan\theta_S|$. The source of such a asymmetry comes from the expressions of $\Gamma_{s \rightarrow gg}$, $\Gamma_{s \rightarrow \gamma\gamma}$, $\Gamma_{s \rightarrow Z\gamma}$ and $\Gamma_{s \rightarrow ZZ}$, which are presented from Eq.(7) to Eq.(16).

In Table II, we show the detailed information for one of the best points in the left and right panels of Fig.2 respectively. In the following, we label the two points by P_1 and P_2 respectively. From this table, one can learn that to explain the diphoton excess in the MDM, the branching ratio of $s \rightarrow \gamma\gamma$ is usually at 1% level, which is significantly larger than that of the Higgs boson in the SM. One can also learn that for the best points, $s \rightarrow gg$ may be either dominant or subdominant decay channel of the s .

Finally, we study the correlations between the diphoton rate at the 13TeV LHC with the rates of the ZZ , WW^* , hh and $t\bar{t}$ signals respectively. The results are presented in Fig.3 for the $Q_X = \frac{2}{3}$ case with the implication of the figure explained in its caption. This figure reveals following

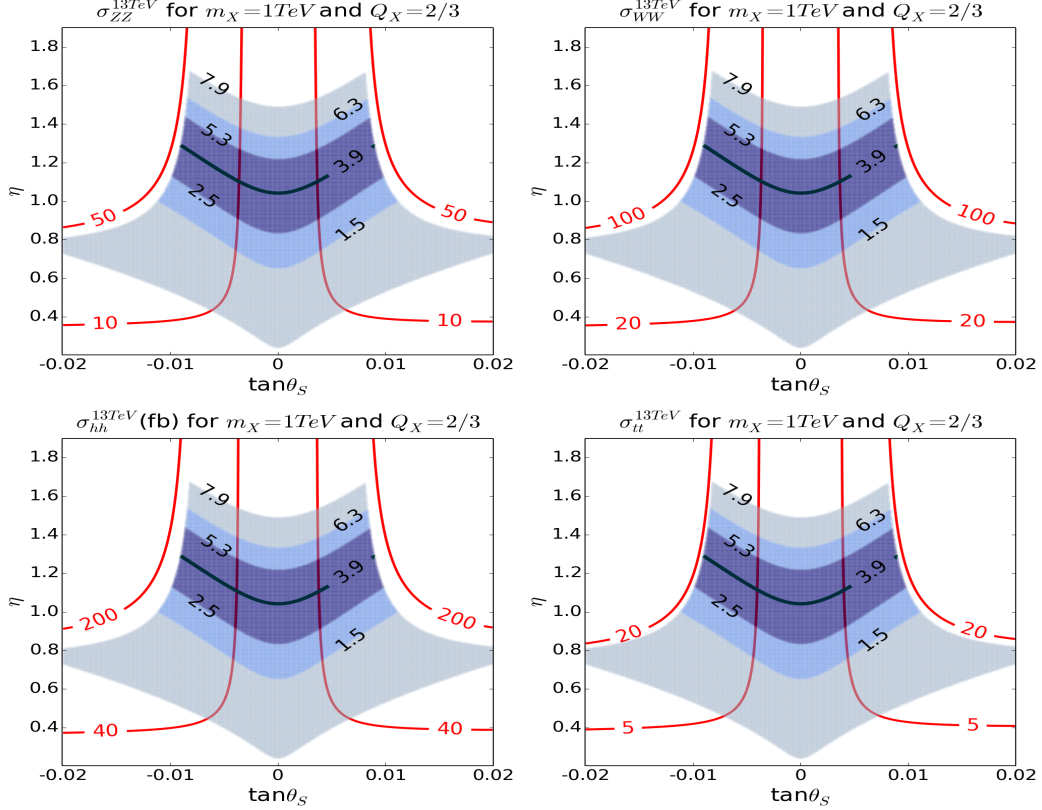


FIG. 3. Correlations of the diphoton rate at the 13TeV with those of ZZ , WW^* , hh and $t\bar{t}$ signals respectively for the $Q_X = \frac{2}{3}$ case, which are shown on the $\eta - \tan\theta_S$ planes. Colors in this figure have same meanings as those in Fig.2, and from the left to right and upper to lower panels, the constant contours (red lines) of the production rates for ZZ , WW^* , hh and $t\bar{t}$ signals are shown respectively. The numbers on the red lines represent the corresponding production rates at the 13TeV LHC. Note that the correlations of the diphoton rate with those of the gg and $Z\gamma$ signals are presented in Eq.(23).

information

- Current LHC data have put upper limits on the rates of the different signals at the 13 – TeV LHC, which are $\sigma_{ZZ} \lesssim 48\text{fb}$, $\sigma_{WW} \lesssim 96\text{fb}$, $\sigma_{hh} \lesssim 190\text{fb}$ and $\sigma_{t\bar{t}} \lesssim 19\text{fb}$.
- Since for a moderately small $\sin\theta_S$, the sZZ , sWW , shh and $st\bar{t}$ couplings are roughly proportional to $\sin\theta_S \simeq \tan\theta_S$, the constant contours of the signal rates exhibit similar behaviors on the $\eta - \tan\theta_S$ plane. Obviously, if the diphoton excess persists at future LHC experiments and meanwhile none of the other signals is observed, a small $\tan\theta_S$ is preferred.
- More important, if more than one type of the signals are measured at the future LHC experiments, one can decide the parameters of the MDM. For example, given that $\sigma_{\gamma\gamma}$ and σ_{jj} are precisely known, one can get the value of Q_X , and if $\sigma_{\gamma\gamma}$ and σ_{ZZ} are also measured,

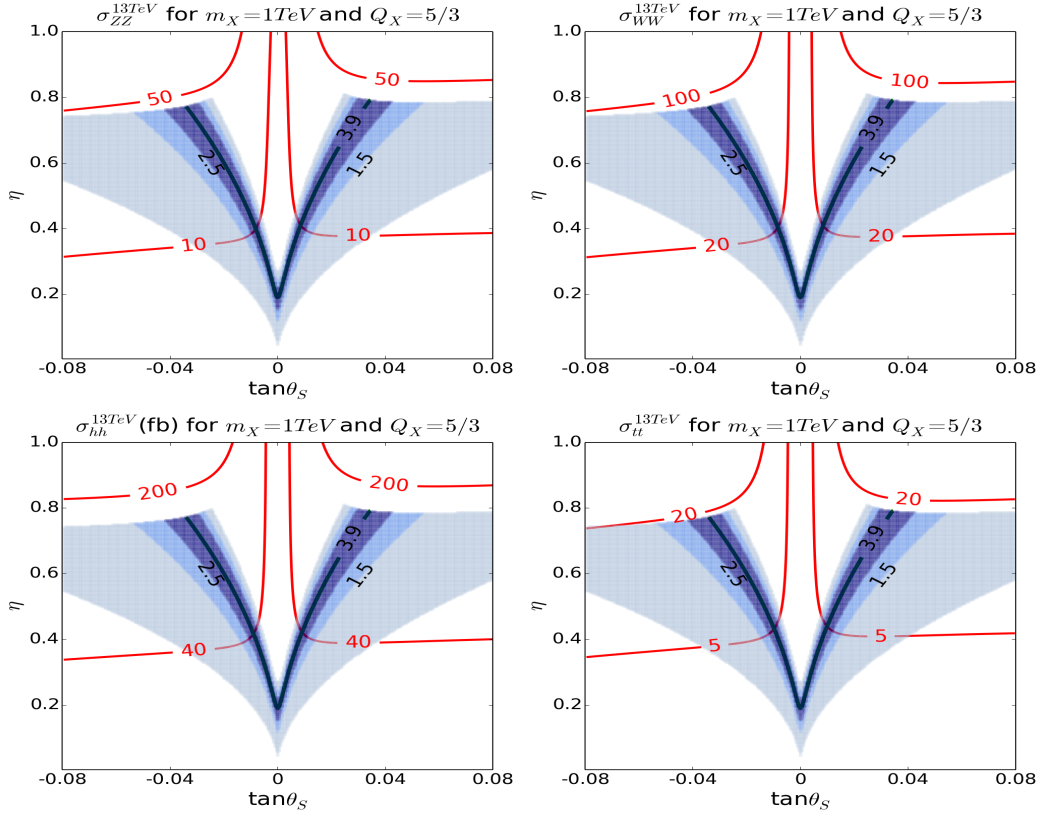


FIG. 4. Similar to Fig.3, but for the $Q_X = \frac{5}{3}$ case.

TABLE III. The scale where the vacuum becomes unstable for different choice of the vector-like fermion number N_X . Here the scale μ is in unit of GeV, and the points P_1 and P_2 correspond to the two benchmark points in Table II. We checked that for the point P_2 with $N_X = 5, 6$, the vacuum keeps stable before λ_H reaches its Landau poles, which are roughly at 5.6×10^{11} GeV and 3.8×10^{10} GeV respectively. We also checked that for the P_2 with $N_X = 4$, the Landau pole of λ_H is roughly at 2.2×10^{13} GeV.

Point	$\mu(N_X = 1)$	$\mu(N_X = 2)$	$\mu(N_X = 3)$	$\mu(N_X = 4)$	$\mu(N_X = 5)$	$\mu(N_X = 6)$
P_1	1000	1000	1000	1015	1180	1350
P_2	1000	4930	57950	2.1×10^7	—	—

one can pin down the favored regions of η and $\sin \theta_S$.

In Fig.4, we show the correlations of the different signals for the $Q_X = \frac{5}{3}$ case. The features of this figure are quite similar to those of Fig.3 except that: i) now the diphoton rate becomes more sensitive to η and $\sin \theta_S$, So to extract the values of the two parameters in this case, a more precise measurement of the diphoton signal is needed. ii) the asymmetry between $\pm \tan \theta_S$ on the rates at 13TeV LHC becomes more obvious.

V. VACUUM STABILITY AT HIGH ENERGY SCALE

About one week before we finish this work, several papers appeared to discuss the vacuum stability in a theoretical framework which is quite similar to the MDM [16–18]. The main argument of these papers was that, in order to explain the diphoton excess, the Yukawa coupling y_X must be so large that the vacuum becomes unstable at a certain high energy scale ². In our opinion, the MDM may be free of this problem due to following two reasons. One is that the MDM is actually a low energy effective theory describing the breakdown of a strong dynamics with approximate scale invariance. This means that the physics beyond the MDM must appear at a certain high energy scale. The other is that, as we emphasized in Section III, the diphoton excess actually imposes non-trivial requirements on the parameter $\eta \equiv \frac{vN_X}{f}$, instead of on the Yukawa coupling $y_X \equiv \frac{\eta m_X}{vN_X}$ directly. For a given value of η , one may increase N_X to suppress the Yukawa coupling y_X , and thus alleviate the problem. In order to verify our speculation, we assume that there are no particles in the strong interaction sector other than the vector-like fermions, and consider the two benchmark points presented in Table II. We repeat the analysis in [18], i.e. we use the same RGEs as those in [18] to run all parameters in the MDM, and also consider the threshold correction to λ_S at the scale m_X . In Table III, we present the scale where the vacuum becomes unstable for different choices of N_X . This table indicates that moderately large N_X and Q_X are helpful to stabilize the vacuum state.

Finally, we remind that, although large Q_X and/or N_X are welcomed to explain the excess, they can not be arbitrarily large in the extension of the SM by one gauge singlet scalar and the vector-like fermions. The reason is that the β function of the gauge coupling g_1 is given by $\beta_{g_1} = (\frac{41}{10} + N_X Q_X^2 \frac{12}{5})g_1^3$ [18], and consequently g_1 increases rapidly with the RGE energy scale for large N_X and Q_X . In this case, the β function of λ_H is dominated by the term proportional to g_1^4 , and consequently, λ_H may reach its Landau pole at an energy scale not far above the weak scale.

VI. CONCLUSION

The MDM extends the SM by adding vector-like fermions and one gauge singlet scalar, which represents a linearized dilaton field. In this theory, the couplings of the dilaton to gg and $\gamma\gamma$ are induced by the loops of the vector-like fermions, and may be sizable in comparison with the Hgg

² The large Yukawa coupling Y_X can influence the vacuum stability condition $4\lambda_H\lambda_S - \lambda_{HS}^2 > 0$ by two ways [18]. One is that it pulls down the value of λ_S in its evolution with the energy scale by the renormalization group equation (RGE). The other is that the threshold correction to the λ_S at the scale m_X is proportional to $-y_X^4$, and consequently λ_S usually becomes negative after considering the correction.

and $H\gamma\gamma$ couplings in the SM. On the other hand, due to the singlet nature of the dilaton its decays into the other SM particles are suppressed. These characters make the diphoton signal of the dilaton potentially detectable at the LHC.

In this work, we tried to interpret the diphoton excess recently reported by the ATLAS and CMS collaborations at the 13 TeV LHC in the framework of the MDM. For this purpose, we first showed by analytic formulae that the production rates of the $\gamma\gamma$, gg , $Z\gamma$, ZZ , WW^* , $t\bar{t}$ and hh signals at the 750GeV resonance are only sensitive to the dilaton-Higgs mixing angle θ_S and the parameter $\eta \equiv vN_X/f$, where N_X denotes the number of the vector-like fermions and f is the dilaton decay constant. Then we scanned the two parameters to find the solutions to the excess. During the scan, we considered various theoretical and experimental constraints, which included the vacuum stability and the perturbativity of the theory at the scale of m_s , the electroweak precision data, the 125GeV Higgs data, the LHC searches for exotic quarks, and the upper bounds on the rates of ZZ , WW^* , $Z\gamma$, $t\bar{t}$ and hh signals at LHC Run I. We concluded that the model can predict the central value of the diphoton rate without conflicting with any constraints. Moreover, after deciding the parameter space for the excess we discussed the signatures of the theory at the LHC Run II. We showed that the rates of the WW^* and hh signals may still reach about 100 fb and 200 fb respectively at the 13 TeV LHC, and thus they provide good prospect for detection in future.

As an indispensable part of this work, we also discussed the vacuum stability of the theory at high energy scales. We showed that, by choosing moderately large N_X and Q_X , the vacuum in our explanation can retain stable up to 10^{11}GeV .

Note added: When we finished this work at the beginning of this January, we noted that two papers had appeared trying to explain the diphoton excess with the dilaton field [14, 15]. However, after reading these papers, we learned that the paper [14] considered the traditional dilaton model, and the paper [15] focused on 5D warped models. So their studies are quite different from ours. We also noted that by then there existed several papers studying the diphoton excess in the model which extends the SM by one gauge singlet scalar field and vector-like fermions [10, 16, 18]. Compared with these works, our study has following features (improvements):

- We considered a generic model which predicts N_X vector-like fermions (by contrast, most of the previous studies considered the most economical $N_X = 1$ case). This enables us to explain the diphoton excess without invoking a large Yukawa coupling y_X . Such a treatment, as we have discussed in section V, is helpful to retain vacuum stability of the theory at high

energy scales.

- More important, by assuming that the dilaton field is fully responsible for the masses of the vector-like fermions, we showed by analytic formulae that the rates for all the signals discussed in this work, such as $\gamma\gamma$, gg , $Z\gamma$, VV^* , $f\bar{f}$ and hh , are only sensitive to the parameter $\eta = \frac{vN_X}{f}$, the dilaton-Higgs mixing angle θ_S and the electric charge of the fermions Q_X . This observation can greatly simplify the analysis on the diphoton excess, and within our knowledge, it was not paid due attention in previous studies.
- We considered various constraints on the model, especially those from different observations at the LHC Run I (which were listed in Table I), and we concluded that the hh signal usually puts the tightest constraint on our explanation. This conclusion is rather new. Moreover, we also studied the signatures of our explanation at the LHC Run II, which are helpful to decide the parameters of the model. Such a study was absent in previous literatures.

Before we end this work, we'd like to clarify its relation with our previous work [13], where we utilized the singlet extension of the Manohar-Wise model to explain the diphoton excess. In either of the works, the scalar sector of the considered model contains a doublet and a singlet scalar field, which mix to form a 125 GeV SM-like Higgs h and a 750 GeV new scalar s , and the $s\gamma\gamma$ and sgg interactions are induced by colored particles through loop effects. In organizing these works, we first introduced the theoretical framework and listed the formula for the partial widths of the scalar s , then we analyzed various constraints on the model and discussed the diphoton signal from the process $gg \rightarrow s \rightarrow \gamma\gamma$. We concluded that both the models can predict the central value of the excess in their vast parameter space. Since the two works adopted same χ^2 function for the excess which only depends on the diphoton rate, the χ^2 values for the best points are same in the two explanations. In spite of these similarities, we still think that the two works are independent since they are based on different physics. The differences are reflected in following aspects:

- The origin of the singlet dominated scalar s . In the work [13], the singlet field is imposed by hand and only for interpreting the excess, while in this work it corresponds to a linearized dilation field, which is well motivated by the broken of a strong dynamic with approximate scale invariance.
- The mechanism to generate sizable $s\gamma\gamma$ and sgg interactions. In the singlet extension of the Manohar-Wise model, these interactions are induced by color-octet and isospin-doublet scalars S_R^A , S_I^A and S_\pm^A with $A = 1, \dots, 8$ denoting color index (Note that there are totally

32 bosonic freedom), so their coupling strengths are proportional to $(C_{sS_i^{A*}S_i^A v})/m_{S_i}^2 A_0(\tau_{S_i})$ with $C_{sS_i^{A*}S_i^A}$ denoting the coupling coefficient for the $sS_i^{A*}S_i^A$ interaction. As a comparison, the couplings in this work are induced by the vector-like fermions, and their strengths are determined by the factor $\eta A_{\frac{1}{2}}(\tau_X)$. Since the loop function A_0 is usually several times smaller than the function $A_{\frac{1}{2}}$ [25], beside the large bosonic freedom, large $C_{sS_i^{A*}S_i^A}$ and meanwhile moderately light S_i^A are also necessary to get the same sizes of the strengths as those in this work. By contrast, we only need to tune the value η to get the right couplings for the excess in this work. So the explanation presented in here is rather simple and straightforward.

- The intrinsic features of the explanations. Due to the particle assignments of the models, the two explanations exhibit different features. For example, for the explanation in [13] the upper limit of the dijet channel in Table I has constrained the diphoton rate to be less than about 7.5fb [13, 47], while in the present work the constraint from the dijet channel on the rate is rather loose. Another example is that for the explanation in [13], the vacuum stability can never constrain the model parameters, while in this work it acts as a main motivation to consider moderately large N_X and Q_X to keep the vacuum stability.

ACKNOWLEDGEMENT

We thank Prof. C. P. Yuan and Fei Wang for helpful discussion, and this work was supported in part by the National Natural Science Foundation of China (NNSFC) under Grant No. 11547103, 11275245, 11547310, 11575053. Dr. Zhu thanks the support of the U.S. National Science Foundation under Grant No. PHY-0855561, while he was working at Michigan State University.

-
- [1] [ATLAS Collaboration], Phys. Lett. B **710** (2012) 49 [arXiv:1202.1408 [hep-ex]].
 - [2] [CMS Collaboration], Phys. Lett. B **710** (2012) 26 [arXiv:1202.1488 [hep-ex]].
 - [3] [ATLAS Collaboration], Phys. Lett. B **716** (2012) 1 [arXiv:1207.7214 [hep-ex]].
 - [4] [CMS Collaboration], Phys. Lett. B **716** (2012) 30 [arXiv:1207.7235 [hep-ex]].
 - [5] [ATLAS collaboration], ATLAS-CONF-2015-081.
 - [6] [CMS Collaboration], collisions at 13TeV,” CMS-PAS-EXO-15-004.
 - [7] M. R. Buckley, arXiv:1601.04751 [hep-ph].
 - [8] S. Dittmaier *et al.* [LHC Higgs Cross Section Working Group Collaboration], arXiv:1101.0593 [hep-ph].
 - [9] D. Buttazzo, A. Greljo and D. Marzocca, arXiv:1512.04929 [hep-ph].
 - [10] A. Falkowski, O. Slone and T. Volansky, arXiv:1512.05777 [hep-ph].

- [11] K. Harigaya and Y. Nomura, arXiv:1512.04850 [hep-ph]; Y. Mambrini, G. Arcadi and A. Djouadi, arXiv:1512.04913 [hep-ph]; M. Backovic, A. Mariotti and D. Redigolo, arXiv:1512.04917 [hep-ph]; A. Angelescu, A. Djouadi and G. Moreau, arXiv:1512.04921 [hep-ph]; Y. Nakai, R. Sato and K. Tobioka, arXiv:1512.04924 [hep-ph]; S. Knapen, T. Melia, M. Papucci and K. Zurek, arXiv:1512.04928 [hep-ph]; A. Pilaftsis, arXiv:1512.04931 [hep-ph]; R. Franceschini *et al.*, arXiv:1512.04933 [hep-ph]; S. Di Chiara, L. Marzola and M. Raidal, arXiv:1512.04939 [hep-ph]; T. Higaki, K. S. Jeong, N. Kitajima and F. Takahashi, arXiv:1512.05295 [hep-ph]; S. D. McDermott, P. Meade and H. Ramani, arXiv:1512.05326 [hep-ph]; J. Ellis, S. A. R. Ellis, J. Quevillon, V. Sanz and T. You, arXiv:1512.05327 [hep-ph]; M. Low, A. Tesi and L. T. Wang, arXiv:1512.05328 [hep-ph]; R. S. Gupta, S. Jger, Y. Kats, G. Perez and E. Stamou, arXiv:1512.05332 [hep-ph]; C. Petersson and R. Torre, arXiv:1512.05333 [hep-ph]; E. Molinaro, F. Sannino and N. Vignaroli, arXiv:1512.05334 [hep-ph]; B. Dutta, Y. Gao, T. Ghosh, I. Gogoladze and T. Li, arXiv:1512.05439 [hep-ph]; Q. H. Cao, Y. Liu, K. P. Xie, B. Yan and D. M. Zhang, arXiv:1512.05542 [hep-ph]; S. Matsuzaki and K. Yamawaki, arXiv:1512.05564 [hep-ph]; A. Kobakhidze, F. Wang, L. Wu, J. M. Yang and M. Zhang, arXiv:1512.05585 [hep-ph]; C. P. D. Harman and S. J. Huber, arXiv:1512.05611 [hep-ph]; R. Martinez, F. Ochoa and C. F. Sierra, arXiv:1512.05617 [hep-ph]; P. Cox, A. D. Medina, T. S. Ray and A. Spray, arXiv:1512.05618 [hep-ph]; D. Becirevic, E. Bertuzzo, O. Sumensari and R. Z. Funchal, arXiv:1512.05623 [hep-ph]; P. Fayet, arXiv:1512.05628 [hep-ph]; J. M. No, V. Sanz and J. Setford, arXiv:1512.05700 [hep-ph]; S. V. Demidov and D. S. Gorbunov, arXiv:1512.05723 [hep-ph]; W. Chao, R. Huo and J. H. Yu, arXiv:1512.05738 [hep-ph]; S. Fichet, G. von Gersdorff and C. Royon, arXiv:1512.05751 [hep-ph]; D. Curtin and C. B. Verhaaren, arXiv:1512.05753 [hep-ph]; L. Bian, N. Chen, D. Liu and J. Shu, arXiv:1512.05759 [hep-ph]; J. Chakraborty, A. Choudhury, P. Ghosh, S. Mondal and T. Srivastava, arXiv:1512.05767 [hep-ph]; A. Ahmed, B. M. Dillon, B. Grzadkowski, J. F. Gunion and Y. Jiang, arXiv:1512.05771 [hep-ph]; P. Agrawal, J. Fan, B. Heidenreich, M. Reece and M. Strassler, arXiv:1512.05775 [hep-ph]; C. Csaki, J. Hubisz and J. Terning, arXiv:1512.05776 [hep-ph]; D. Aloni, K. Blum, A. Dery, A. Efrati and Y. Nir, arXiv:1512.05778 [hep-ph]; Y. Bai, J. Berger and R. Lu, arXiv:1512.05779 [hep-ph]; E. Gabrielli, K. Kannike, B. Mele, M. Raidal, C. Spethmann and H. Veerm, arXiv:1512.05961 [hep-ph]; R. Benbrik, Chuan-Hung Chen, Takaaki Nomura, arXiv:1512.06028 [hep-ph]; J. S. Kim, J. Reuter, K. Rolbiecki and R. R. de Austri, arXiv:1512.06083 [hep-ph]; A. Alves, A. G. Dias and K. Sinha, arXiv:1512.06091 [hep-ph]; L. M. Carpenter, R. Colburn and J. Goodman, arXiv:1512.06107 [hep-ph]; J. Bernon and C. Smith, arXiv:1512.06113 [hep-ph]; W. Chao, arXiv:1512.06297 [hep-ph]; M. T. Arun and P. Saha, arXiv:1512.06335 [hep-ph]; C. Han, H. M. Lee, M. Park and V. Sanz, arXiv:1512.06376 [hep-ph]; I. Chakraborty and A. Kundu, arXiv:1512.06508 [hep-ph]; H. Han, S. Wang and S. Zheng, arXiv:1512.06562 [hep-ph]; X. F. Han and L. Wang, arXiv:1512.06587 [hep-ph]; M. x. Luo, K. Wang, T. Xu, L. Zhang and G. Zhu, arXiv:1512.06670 [hep-ph]; J. Chang, K. Cheung and C. T. Lu, arXiv:1512.06671 [hep-ph]; D. Bardhan, D. Bhatia, A. Chakraborty, U. Maitra, S. Raychaudhuri and T. Samui, arXiv:1512.06674 [hep-ph]; T. F. Feng, X. Q. Li, H. B. Zhang and S. M. Zhao, arXiv:1512.06696 [hep-ph]; O. Antipin,

M. Mojaza and F. Sannino, arXiv:1512.06708 [hep-ph]; F. Wang, L. Wu, J. M. Yang and M. Zhang, arXiv:1512.06715 [hep-ph]; F. P. Huang, C. S. Li, Z. L. Liu and Y. Wang, arXiv:1512.06732 [hep-ph]; W. Liao and H. q. Zheng, arXiv:1512.06741 [hep-ph]; J. J. Heckman, arXiv:1512.06773 [hep-ph]; X. J. Bi, Q. F. Xiang, P. F. Yin and Z. H. Yu, arXiv:1512.06787 [hep-ph]; J. S. Kim, K. Rolbieceki and R. R. de Austri, arXiv:1512.06797 [hep-ph]; L. Berthier, J. M. Cline, W. Shepherd and M. Trott, arXiv:1512.06799 [hep-ph]; W. S. Cho, D. Kim, K. Kong, S. H. Lim, K. T. Matchev, J. C. Park and M. Park, arXiv:1512.06824 [hep-ph]; J. M. Cline and Z. Liu, arXiv:1512.06827 [hep-ph]; M. Bauer and M. Neubert, arXiv:1512.06828 [hep-ph]; M. Chala, M. Duerr, F. Kahlhoefer and K. Schmidt-Hoberg, arXiv:1512.06833 [hep-ph]; K. Kulkarni, arXiv:1512.06836 [hep-ph]; D. Barducci, A. Goudelis, S. Kulkarni and D. Sengupta, arXiv:1512.06842 [hep-ph]; S. M. Boucenna, S. Morisi and A. Vicente, arXiv:1512.06878 [hep-ph]; C. W. Murphy, arXiv:1512.06976 [hep-ph]; A. E. C. Hernández and I. Nisandzic, arXiv:1512.07165 [hep-ph]; U. K. Dey, S. Mohanty and G. Tomar, arXiv:1512.07212 [hep-ph]; G. M. Pelaggi, A. Strumia and E. Vigiani, arXiv:1512.07225 [hep-ph]; J. de Blas, J. Santiago and R. Vega-Morales, arXiv:1512.07229 [hep-ph]; A. Belyaev, G. Cacciapaglia, H. Cai, T. Flacke, A. Parolini and H. Serôdio, arXiv:1512.07242 [hep-ph]; P. S. B. Dev and D. Teresi, arXiv:1512.07243 [hep-ph]; W. C. Huang, Y. L. S. Tsai and T. C. Yuan, arXiv:1512.07268 [hep-ph]; S. Moretti and K. Yagyu, arXiv:1512.07462 [hep-ph]; K. M. Patel and P. Sharma, arXiv:1512.07468 [hep-ph]; M. Badziak, arXiv:1512.07497 [hep-ph]; S. Chakraborty, A. Chakraborty and S. Raychaudhuri, arXiv:1512.07527 [hep-ph]; Q. H. Cao, S. L. Chen and P. H. Gu, arXiv:1512.07541 [hep-ph]; W. Altmannshofer, J. Galloway, S. Gori, A. L. Kagan, A. Martin and J. Zupan, arXiv:1512.07616 [hep-ph]; M. Cvetič, J. Halverson and P. Langacker, arXiv:1512.07622 [hep-ph]; J. Gu and Z. Liu, arXiv:1512.07624 [hep-ph]; B. C. Allanach, P. S. B. Dev, S. A. Renner and K. Sakurai, arXiv:1512.07645 [hep-ph]; H. Davoudiasl and C. Zhang, arXiv:1512.07672 [hep-ph]; N. Craig, P. Draper, C. Kilic and S. Thomas, arXiv:1512.07733 [hep-ph]; K. Das and S. K. Rai, arXiv:1512.07789 [hep-ph]; K. Cheung, P. Ko, J. S. Lee, J. Park and P. Y. Tseng, arXiv:1512.07853 [hep-ph]; J. Liu, X. P. Wang and W. Xue, arXiv:1512.07885 [hep-ph]; J. A. Casas, J. R. Espinosa and J. M. Moreno, arXiv:1512.07895 [hep-ph]; L. J. Hall, K. Harigaya and Y. Nomura, arXiv:1512.07904 [hep-ph]; H. Han, S. Wang and S. Zheng, arXiv:1512.07992 [hep-ph]; J. C. Park and S. C. Park, arXiv:1512.08117 [hep-ph]; arXiv:1512.08221 [hep-ph]; D. Chway, R. Dermšek, T. H. Jung and H. D. Kim, arXiv:1512.08221 [hep-ph]; G. Li, Y. n. Mao, Y. L. Tang, C. Zhang, Y. Zhou and S. h. Zhu, arXiv:1512.08255 [hep-ph]; Y. L. Tang and S. h. Zhu, arXiv:1512.08323 [hep-ph]; H. An, C. Cheung and Y. Zhang, arXiv:1512.08378 [hep-ph]; J. Cao, F. Wang and Y. Zhang, arXiv:1512.08392 [hep-ph]; F. Wang, W. Wang, L. Wu, J. M. Yang and M. Zhang, arXiv:1512.08434 [hep-ph]; C. Cai, Z. H. Yu and H. H. Zhang, arXiv:1512.08440 [hep-ph]; Q. H. Cao, Y. Liu, K. P. Xie, B. Yan and D. M. Zhang, arXiv:1512.08441 [hep-ph]; J. E. Kim, arXiv:1512.08467 [hep-ph]; J. Gao, H. Zhang and H. X. Zhu, arXiv:1512.08478 [hep-ph]; W. Chao, arXiv:1512.08484 [hep-ph]; X. J. Bi *et al.*, arXiv:1512.08497 [hep-ph]; L. A. Anchordoqui, I. Antoniadis, H. Goldberg, X. Huang, D. Lust and T. R. Taylor, arXiv:1512.08502 [hep-ph]; P. S. B. Dev, R. N. Mohapatra and Y. Zhang, arXiv:1512.08507

- [hep-ph]; L. E. Ibanez and V. Martin-Lozano, arXiv:1512.08777 [hep-ph]; C. W. Chiang, M. Ibe and T. T. Yanagida, arXiv:1512.08895 [hep-ph]; S. K. Kang and J. Song, arXiv:1512.08963 [hep-ph]; Y. Hamada, T. Noumi, S. Sun and G. Shiu, arXiv:1512.08984 [hep-ph]; X. J. Huang, W. H. Zhang and Y. F. Zhou, arXiv:1512.08992 [hep-ph]; S. Kanemura, K. Nishiwaki, H. Okada, Y. Orikasa, S. C. Park and R. Watanabe, arXiv:1512.09048 [hep-ph]; S. Kanemura, N. Machida, S. Odori and T. Shindou, arXiv:1512.09053 [hep-ph]; I. Low and J. Lykken, arXiv:1512.09089 [hep-ph]; A. E. C. Hernández, arXiv:1512.09092 [hep-ph]; Y. Jiang, Y. Y. Li and T. Liu, arXiv:1512.09127 [hep-ph]; K. Kaneta, S. Kang and H. S. Lee, arXiv:1512.09129 [hep-ph]; L. Marzola, A. Racioppi, M. Raidal, F. R. Urban and H. Veermäe, arXiv:1512.09136 [hep-ph]; E. Ma, arXiv:1512.09159 [hep-ph]; A. Dasgupta, M. Mitra and D. Borah, arXiv:1512.09202 [hep-ph]; S. Jung, J. Song and Y. W. Yoon, arXiv:1601.00006 [hep-ph]; C. T. Potter, arXiv:1601.00240 [hep-ph]; T. Nomura and H. Okada, arXiv:1601.00386 [hep-ph]; P. Ko, Y. Omura and C. Yu, arXiv:1601.00586 [hep-ph]; X. F. Han, L. Wang, L. Wu, J. M. Yang and M. Zhang, arXiv:1601.00534 [hep-ph]; K. Ghorbani and H. Ghorbani, arXiv:1601.00602 [hep-ph]; U. Danielsson, R. Enberg, G. Ingelman and T. Mandal, arXiv:1601.00624 [hep-ph]; W. Chao, arXiv:1601.00633 [hep-ph]; C. Csaki, J. Hubisz, S. Lombardo and J. Terning, arXiv:1601.00638 [hep-ph]; A. Karozas, S. F. King, G. K. Leontaris and A. K. Meadowcroft, arXiv:1601.00640 [hep-ph]; A. E. C. Hernández, I. d. M. Varzielas and E. Schumacher, arXiv:1601.00661 [hep-ph]; T. Modak, S. Sadhukhan and R. Srivastava, arXiv:1601.00836 [hep-ph]; B. Dutta, Y. Gao, T. Ghosh, I. Gogoladze, T. Li, Q. Shafi and J. W. Walker, arXiv:1601.00866 [hep-ph]; F. F. Deppisch, C. Hati, S. Patra, P. Pritimita and U. Sarkar, arXiv:1601.00952 [hep-ph]; H. Ito, T. Moroi and Y. Takaesu, arXiv:1601.01144 [hep-ph]; H. Zhang, arXiv:1601.01355 [hep-ph]; A. Berlin, arXiv:1601.01381 [hep-ph]; S. Bhattacharya, S. Patra, N. Sahoo and N. Sahu, arXiv:1601.01569 [hep-ph]; F. D’Eramo, J. de Vries and P. Panci, arXiv:1601.01571 [hep-ph]; I. Sahin, arXiv:1601.01676 [hep-ph]; S. Fichet, G. von Gersdorff and C. Royon, arXiv:1601.01712 [hep-ph]; D. Borah, S. Patra and S. Sahoo, arXiv:1601.01828 [hep-ph]; D. Stolarski and R. Vega-Morales, arXiv:1601.02004 [hep-ph].
- [12] F. Goertz, J. F. Kamenik, A. Katz and M. Nardecchia, arXiv:1512.08500 [hep-ph].
- [13] J. Cao, C. Han, L. Shang, W. Su, J. M. Yang and Y. Zhang, Phys. Lett. B **755**, 456 (2016) [arXiv:1512.06728 [hep-ph]].
- [14] B. Bellazzini, R. Franceschini, F. Sala and J. Serra, arXiv:1512.05330 [hep-ph];
- [15] E. Megias, O. Pujolas and M. Quiros, arXiv:1512.06106 [hep-ph].
- [16] J. Zhang and S. Zhou, arXiv:1512.07889 [hep-ph].
- [17] M. Dhuria and G. Goswami, arXiv:1512.06782 [hep-ph].
- [18] M. Son and A. Urbano, arXiv:1512.08307 [hep-ph].
- [19] A. Salvio and A. Mazumdar, arXiv:1512.08184 [hep-ph].
- [20] T. Abe *et al.*, Phys. Rev. D **86** (2012) 115016.
- [21] T. Abe *et al.*, EPJ Web Conf. **49** (2013) 15018.
- [22] J. Cao, Y. He, P. Wu, M. Zhang and J. Zhu, JHEP **1401** (2014) 150 [arXiv:1311.6661 [hep-ph]].

- [23] R. Foot, A. Kobakhidze and R. R. Volkas, Phys. Lett. B **655** (2007) 156;
 W. D. Goldberger, B. Grinstein and W. Skiba, Phys. Rev. Lett. **100** (2008) 111802;
 J. Fan, W. D. Goldberger, A. Ross and W. Skiba, Phys. Rev. D **79** (2009) 035017;
 R. Foot, A. Kobakhidze and K. L. McDonald, Eur. Phys. J. C **68** (2010) 421;
 V. Barger, M. Ishida and W. -Y. Keung, Phys. Rev. Lett. **108** (2012) 101802;
 B. Coleppa, T. Gregoire and H. E. Logan, Phys. Rev. D **85** (2012) 055001;
 V. Barger, M. Ishida and W. -Y. Keung, Phys. Rev. D **85** (2012) 015024.
- [24] C. T. Hill, Phys. Lett. B **266**, 419 (1991).
- [25] A. Djouadi, Phys. Rept. **457** (2008) 1 [hep-ph/0503172]; Phys. Rept. **459** (2008) 1 [hep-ph/0503173].
- [26] [ATLAS Collaboration], Phys. Rev. D **91** (2015) 11, 112011 [arXiv:1503.05425 [hep-ex]].
- [27] [ATLAS Collaboration], JHEP **1508** (2015) 105 [arXiv:1505.04306 [hep-ex]].
- [28] [CMS Collaboration], CMS-PAS-B2G-15-006.
- [29] <https://twiki.cern.ch/twiki/bin/view/LHCPhysics/CERNYellowReportPageAt1314TeV>
- [30] M. E. Peskin and T. Takeuchi, Phys. Rev. D **46** (1992) 381.
- [31] M. Baak *et al.* [Gfitter Group Collaboration], Eur. Phys. J. C **74** (2014) 3046 [arXiv:1407.3792 [hep-ph]].
- [32] <https://atlas.web.cern.ch/Atlas/GROUPS/PHYSICS/CombinedSummaryPlots/HIGGS/>
- [33] <https://twiki.cern.ch/twiki/bin/view/CMSPublic/PhysicsResultsHIG>
- [34] J. Cao, F. Ding, C. Han, J. M. Yang and J. Zhu, JHEP **1311** (2013) 018 [arXiv:1309.4939 [hep-ph]].
- [35] [ATLAS Collaboration], Phys. Rev. D **91**, no. 5, 052007 (2015) [arXiv:1407.1376 [hep-ex]].
- [36] CMS Collaboration [CMS Collaboration], CMS-PAS-EXO-14-005.
- [37] [CMS Collaboration], Phys. Lett. B **749** (2015) 560 [arXiv:1503.04114 [hep-ex]].
- [38] [ATLAS Collaboration], Phys. Rev. D **92** (2015) 092004 [arXiv:1509.04670 [hep-ex]].
- [39] [ATLAS Collaboration], Phys. Rev. Lett. **114**, no. 8, 081802 (2015) [arXiv:1406.5053 [hep-ex]].
- [40] [ATLAS Collaboration], Eur. Phys. J. C **75**, no. 9, 412 (2015) [arXiv:1506.00285 [hep-ex]].
- [41] [CMS Collaboration], JHEP **1510**, 144 (2015) [arXiv:1504.00936 [hep-ex]].
- [42] [ATLAS Collaboration], arXiv:1509.00389 [hep-ex].
- [43] [ATLAS Collaboration], arXiv:1507.05930 [hep-ex].
- [44] [ATLAS Collaboration], Phys. Lett. B **738**, 428 (2014) [arXiv:1407.8150 [hep-ex]].
- [45] [CMS Collaboration], arXiv:1506.03062 [hep-ex].
- [46] [ATLAS Collaboration], JHEP **1508**, 148 (2015) [arXiv:1505.07018 [hep-ex]].
- [47] F. Staub *et al.*, arXiv:1602.05581 [hep-ph].